Bioinspiration & Biomimetics

PAPER • OPEN ACCESS

Should friction losses be included in an electromechanical model of a bioinspired flapping-wing micro aerial vehicle to estimate the flight energetic requirements?

To cite this article: Moonsoo Park *et al* 2022 *Bioinspir. Biomim.* **17** 036011

View the article online for updates and enhancements.

You may also like

- Quasi-steady aerodynamic model of clap-and-fling flapping MAV and validation using free-flight data
S F Armanini, J V Caetano, G C H E de Croon et al.

- Design and stable flight of a 21 g insect-like tailless flapping wing micro air vehicle with angular rates feedback control
Hoang Vu Phan, Taesam Kang and Hoon Cheol Park

- Experimental optimization of wing shape for a hummingbird-like flapping wing micro air vehicle
Yanghai Nan, Matj Karásek, Mohamed Esseghir Lalami et al.

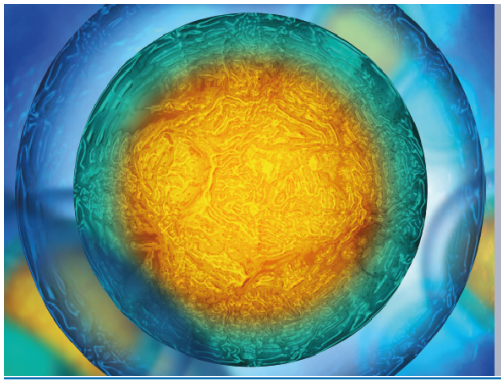

Biophysical Society IOP ebooks™

Your publishing choice in all areas of biophysics research.

Start exploring the collection–download the first chapter of every title for free.

This content was downloaded from IP address 128.41.35.152 on 01/07/2022 at 14:14

Bioinspiration & Biomimetics

OPEN ACCESS

RECEIVED
2 November 2021

REVISED
23 December 2021

ACCEPTED FOR PUBLICATION
1 March 2022

PUBLISHED
22 April 2022

Original content from this work may be used under the terms of the Creative Commons Attribution 4.0 licence.

Any further distribution of this work must maintain attribution to the author(s) and the title of the work, journal citation and DOI.

PAPER

Should friction losses be included in an electromechanical model of a bioinspired flapping-wing micro aerial vehicle to estimate the flight energetic requirements?

Moonsoo Park, Yiannis Ventikos and Ali Abolfathi*

Mechanical Engineering, University College London, London, United Kingdom

* Author to whom any correspondence should be addressed.

E-mail: a.abolfathi@ucl.ac.uk

Keywords: equations of motion, bio-inspired flapping wing micro aerial vehicle, kinetics of flapping mechanism, friction, optimisation

Abstract

The paper aims to examine the effects of mechanical losses on the performance of a bioinspired flapping-wing micro aerial vehicle (FWMAV) and ways to mitigate them by introducing a novel electromechanical model. The mathematical model captures the effect of a DC gear motor, slider-crank, flapping-wings aerodynamics, and frictional losses. The aerodynamic loads are obtained using a quasi-steady flow model. The parameters of the flight mechanism are estimated using published experimental data which are also used to validate the mathematical model. Incorporating the flapping mechanism friction losses into the mathematical model enables capturing the physics of the problem with higher accuracy, which is not possible with simpler models. It also makes it possible to estimate the aerodynamic energetic requirements. Moreover, the model enabled evaluations of the effects of adding bioinspired elastic elements on the efficiency of the system. Although it is established through experimental studies that the addition of a bioinspired elastic element can improve system efficiency and increase lift generation, the existing mathematical models fail to model and predict such effects. It has been demonstrated that the addition of an elastic element can reduce friction losses in the system by decreasing the internal forces. Optimised parameters for a FWMAV incorporating elastic elements are also obtained.

1. Introduction

Flying insects and birds have inspired researchers and engineers to develop flapping-wing aerial vehicles [1–10]. A summary of such systems can be found in [3, 11, 12]. High efficiency, reduced size, flying at low speeds, rapid acceleration, and a high level of manoeuvrability are mentioned as benefits of adapting a flapping-wing system at mini and micro scales [13–17]. At such scales, mathematical modelling of the relevant aerodynamics and kinetics, and accurate fabrications are challenging [18]. Nevertheless, an accurate mathematical model is essential to develop and optimise a flapping-wing micro aerial vehicle (FWMAV). In order to estimate and optimise the energetic requirements of a FWMAV, the mathematical model should account for losses as well as aerodynamic, electric and dynamic loads in the system. Accurate modelling of the former is more difficult for a FWMAV with sliding parts such as those that are using DC motors. This paper introduces an electromechanical model for a DC motor actuated FWMAV that accounts for different forms of energy losses in the system and demonstrates how the model can be used to predict the flight energetic requirements more accurately.

Sepcu [19] derived a mathematical model of a flapping mechanism that has two movable levers driven by a rotary motor. The motor torque was assumed constant in their study. Campolo *et al* [20] designed a flapping system using two DC motors which are controlled to generate reciprocation directly. A mathematical model was developed considering both electrical and mechanical losses in the DC motor, rotor inertia, and aerodynamic load as a quadratic damper. Lau *et al* [14] adopt a slider-crank mechanism with a DC motor to make a FWMAV. A rigid body model and a compliant mechanism are designed, and their mathematical models for static analysis are introduced in [14]. They compared the

© 2022 The Author(s). Published by IOP Publishing Ltd

theoretical values to the experiment results in terms of the input and output power of the motor and the generated thrust. However, a static analysis model does not suit to estimate the dynamics response of the system. Baek *et al* [21] derived non-dimensional kinematic equations for a FWMAV that operates with a slider-crank mechanism and a DC motor. The model includes the electromechanical characteristics of the motor, kinematics of slider-crank and aerodynamic load as a quadratic damper. However, the mathematical model was not used to predict the experimental results but used to understand how parameters affect the motor speed, and the input and output power of the DC motor. Khan *et al* [22] derived equations of motion for a flight mechanism with four-bar linkages driven by a crank. The model captured the effect of wings' stiffness, and inertia and aerodynamic loads were modelled using the blade element theory. The effect of wing stiffness and inertia on the averaged flapping frequency, lift and aerodynamic power were investigated.

Mechanical losses should be considered in the mathematical model to achieve an accurate prediction of the system performance. Yang *et al* [10] and Jeon *et al* [23] state that friction losses can be the dominant factor in estimating the performance of a flapping mechanism. It is also shown that friction losses account for a substantial portion of input power which may be proportional to the power required to overcome inertia loads in a small flapping mechanism [14, 22]. Nevertheless, in most previous studies friction losses are not considered in modelling FWMAVs. An increased aerodynamic load is considered in some models to compensate for the energy losses in the system [20–22]. A viscous damper is used in [24, 25] to model friction losses. In [14, 19], losses are modelled as quadratic damping. Although these models may simulate the energy loss in the system, they may not be suitable for optimisation due to the dependency of the friction losses to the contact force and relative displacement of two surfaces. This may also lead to erroneous results in the estimation of flight energetic requirements. In this paper, the electromechanical model of the FWMAV powered by a rotary motor is presented which also models friction losses. The model is used to demonstrate how the system energetic requirements can be improved by the addition of a potential energy storage element.

In every flapping stroke, wings accelerate at the beginning of the stroke and deaccelerate at the end of it. The inertia forces are of conservative types and there is no net energy transfer to overcome inertia loads in a cycle. The power associated with inertia loads in a flapping-wing mechanism is of a reactive type. However, the increased losses in the system due to increased internal loads and also the lack of a power conversion mechanism in the system may cause an increase in flight energetic requirements [26]. Insects can overcome this problem by storing elastic energy in the flight muscles [27], thorax, and wing hinges [15] and forming a resonance system that cancels out inertia forces in a cycle. In a FWMAV with a rotary motor, the high rotational inertia of the rotor can provide a means to store energy in accelerating and deaccelerating of the wings. However, the increased internal forces due to the inertia loads would increase mechanical losses. Similar to insects, elastic storage energy can be used to minimize the reactive power and reduce the losses in a FWMAV.

Adding springs is one of the simplest and the most common ways to utilise elastic energy storage and to reduce the reactive power in the flapping mechanism. Khan *et al* [22] experimentally showed that adding springs into the wing hinges can increase the aerodynamic power in a crank-rocker flapping mechanism at a certain range of frequency. Madangopal *et al* [28] showed it by simulations that incorporating springs into the design with a crank-rocker mechanism reduces the motor torque variation up to 56.32% and the maximum torque by 12%. Tantanawat and Kota [29] showed via numerical studies that the peak input power can be reduced by 42% by adding a spring in a four-bar flapping mechanism. They attributed that the energy stored in the spring helps the subsequent wing acceleration and deceleration. This results in the reduction of torque variation and peak input power requirements. However, Baek *et al* [21] experimentally showed that adding spring is not always beneficial. Adding linear springs to the slider where wings are connected only saved power above the resonant frequency and they work as an extra payload below the resonant frequency. Thus, it is also important to select optimized springs to maximise energy efficiency.

In this paper, an electromechanical model for a FWMAV comprised of a DC gear motor, slider-crank and wings is developed. Friction losses are modelled using Coulomb's law which is used to demonstrate how the addition of a spring can reduce losses in the system. The model is presented in section 2. A curve fitting approach is used to obtain the parameters of the model based on published measurements in [14] in section 3. The model also made it possible to obtain a more accurate estimate of the aerodynamic power in the reported experimental work. In section 4, it is shown how the addition of spring to cancel inertial loads at resonance can result in an increased efficiency due to a decrease in internal loads and losses associated with them. In section 5, the results of trend analysis are presented and the operating range for the flight mechanism is suggested.

2. Modelling

A slider-crank mechanism can be used to convert the rotary motion of a DC gear motor to a flapping motion. A schematic diagram of such a mechanism is shown in figure 1(a) and can be used to model the

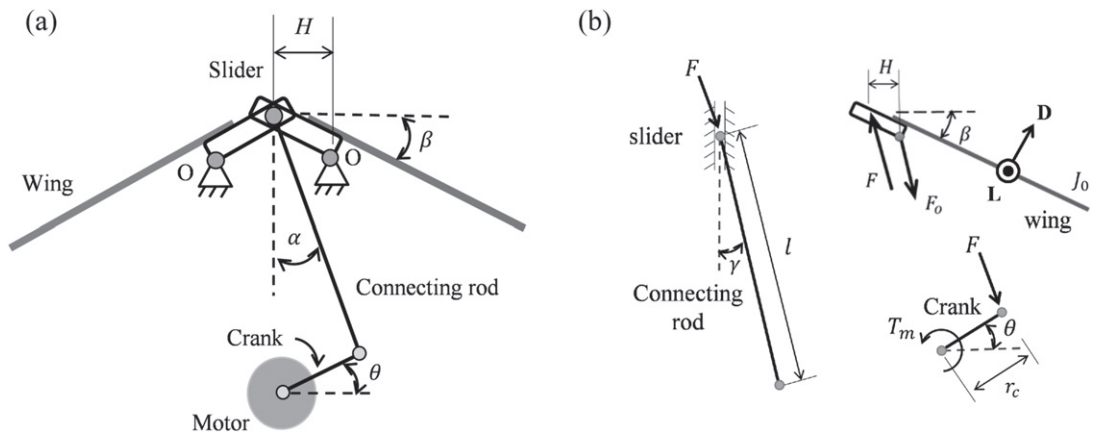

Figure 1. (a) A schematic view of a FWMAV, (b) free body diagram of the wing and the crank and connecting rod, demonstrating the dimensions and the slider path of motion. Reproduced from [30]. Permission granted by authors.

experimental flapping mechanism that is reported in [14]. The free body diagram of the slider-crank mechanism is shown in figure 1(b) where internal forces are shown alongside geometrical parameters. The lift is perpendicular to the leading edge of the wing, and the drag is perpendicular to the wing surface.

By neglecting masses of the connecting rod and the crank, the equation of motion for the wing can be obtained,

$$J_w\ddot{\beta} + \overline{D}\overline{r} = FH\left(\sin\gamma\,\tan\beta + \cos\gamma\right), \quad (1)$$

where J_w is the moment of inertia of the wings about the wing hinge, $\overline{D}$ is the drag, $\overline{r}$ is the distance between the aerodynamic centre and the wing hinge, F is the crank reaction force, H is the horizontal distance between the wing hinge and the slider, β is the wing angle with the horizontal axis, γ is the angle between the connecting rod and the vertical axis. In the above equation, the forces on both wings are considered together. The counter-clockwise rotation is considered positive here.

For modelling aerodynamic load on the wings, blade element theory is used. The quasi-steady approximation allows the estimation of resultant aerodynamic lift, L_r and drag, D_r acting on a sectional area A_r at a distance r from the wing hinge [15],

$$L_r = \frac{1}{2}\rho V_r^2 A_r C_L \quad (2)$$

$$D_r = \frac{1}{2}\rho V_r\left|V_r\right| A_r C_D \quad (3)$$

$$A_r = c(r)\mathrm{d}r, \quad (4)$$

where ρ is the air density of 1.225 kg m^{-3}, V_r is the relative air velocity, C_L and C_D are lift and drag coefficients respectively, and $c(r)$ is the chord length at r.

The motor torque can be obtained as a function of internal force F,

$$T_m = Fr_c\left(\sin\theta\,\sin\gamma + \cos\theta\,\cos\gamma\right) + T_f, \quad (5)$$

where T_m is the motor output torque, T_f is the equivalent torque due to friction losses in the system called friction torque here, r_c is the crank radius, θ is the angle between the crank arm and horizontal axis. The friction forces in the system are a function of the contact forces of two sliding surfaces. The Coulomb friction model can be used to obtain the friction torque T_f as a function of internal loads,

$$T_f = F\mu r_e, \quad (6)$$

where μ is the friction coefficient and r_e is the effective radius. This is used as an overall estimate of friction losses in the sliding parts of the system. The product μr_e can be estimated from experimental data as shown in section 3. Equation (6) enables modelling of the effect of internal loads on losses of the system.

Geared coreless DC motors are small enough to be used for FWMAVs and they are commercially available. The equivalent circuit of a geared coreless DC motor is shown in figure 2.

The characteristic equations of the geared DC motor are,

$$v = L_a\frac{\mathrm{d}i}{\mathrm{d}t} + R_a i + e_{EMF} \quad (7)$$

$$T_2 - T_m = \left(J_G + n^2 J_m\right)\ddot{\theta}_2 + \left(b_G + n^2 b_m\right)\dot{\theta}_2 \quad (8)$$

$$T_1 = K_b i \quad (9)$$

$$T_1\dot{\theta}_1 = T_2\dot{\theta}_2 \quad (10)$$

$$e_{EMF} = K_b\dot{\theta}_1, \quad (11)$$

where v is the applied voltage, i is the armature current, R_a is the armature coil resistance, L_a is the armature coil inductance, e_{EMF} is the back electromotive force, T_1 is the coil torque, T_2 is the coil torque after applying the gear ratio, J_m is the motor inertia, J_G is the gear inertia, $\dot{\theta}_1$ is the motor shaft speed, $\dot{\theta}_2$ is the gear speed, K_b is the motor torque constant, b_m is the

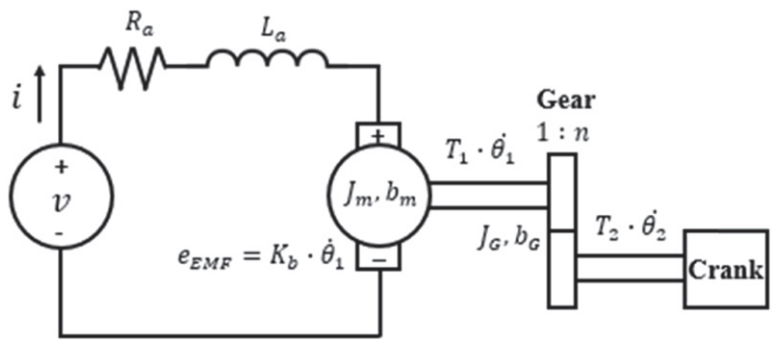

Figure 2. The equivalent circuit of a geared DC motor. Reproduced from [30]. Permission granted by authors.

Table 1. Parameters used for modelling the geared DC motor.

Parameter	Input value
R_a	9Ω
L_a	29×10^{-3} H
K_b	0.01 Nm A^{-1}
$J_G + n^2 J_m$	1.5×10^{-7} kg m^2
$b_G + n^2 b_m$	3.6×10^{-6} Nm s rad^{-1}

mechanical loss coefficient of the motor, n is the gear ratio, and b_G is the gear loss coefficient.

3. Parameter estimation and verification

To estimate the parameters used in the simulation, the measurements reported in [14] are used. A commercial geared coreless DC motor (Precision Microdrive 206-102) is used in the FWMAV of [14]. Apart from the inertia and mechanical loss coefficient, motor parameters are provided by the manufacturer [31]. An initial estimate for motor inertia is obtained by assuming a steel cylinder for the rotor. For the loss coefficient, an initial estimate of 29.6×10^{-9} Nm s rad^{-1} is used [20]. The performance curves provided by the motor manufacturer are used through an iterative process to estimate the inertia and loss coefficient of the gear motor. The motor resistance is also adjusted to replicate the performance curves. The parameters of the geared DC motor that are used in this research are given in table 1.

The wings have a semi-elliptical shape [14]. The shape and the geometric parameters of the wing are shown in figure 3. The lift and drag coefficients can be obtained as functions of the instantaneous angle of attack [32],

$$C_L = 0.225 + 1.58 \times \sin(2.13 \times \alpha - 7.2^\circ) \quad (12)$$

$$C_D = 1.92 - 1.55 \times \cos(2.04 \times \alpha - 9.82^\circ), \quad (13)$$

where α is the angle of attack in degree.

In order to allow passive rotation of wings about the leading edge, the frame at the root chord of the wing is flexible while leading-edge frames are almost

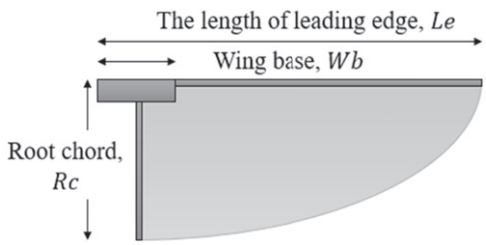

Figure 3. A schematic view of the wing.

rigid. The pitch angle of the wing depends on the wing velocity. However, no information about the instantaneous angle of attack was provided in [14]. The angle of attack is assumed to be a function of the wing angular velocity here,

$$\alpha = 90 - C_\alpha \left(\left| \dot{\beta} \right| \times \frac{360}{2\pi} \right), \quad (14)$$

where C_α is an arbitrary coefficient that is obtained empirically using reported measurements in [14].

The electrical input power and an estimate of motor output power for three different conditions (flapping in the air, in a vacuum and wingless conditions) are reported in [14]. The average electrical input power can be obtained from the following equation,

$$\overline{P_e} = \frac{1}{T} \int_T vi \, dt, \quad (15)$$

where $\overline{P}_e$ is the average electrical input power and T is the period of a flapping cycle. Similarly, the average mechanical output power of the motor can be obtained,

$$\overline{P}_m = \frac{1}{T} \int_T T_m \dot{\theta} dt, \quad (16)$$

where $\overline{P}_m$ is the average motor output power.

In [14], a different estimate of motor output power is used which is defined as,

$$\overline{P}_{m,ref} = 2\pi f K_{b,ref} \overline{I}, \quad (17)$$

where $\overline{P}_{m,ref}$ is assumed the average estimate of motor output power, f is the motor output frequency in Hz which is equal to the wingbeat frequency, $\overline{I}$ is average

current, and the torque constant, $K_{b\cdot ref}$, assumed to be 7.664×10^{-3} Nm A^{-1}. To prevent confusion with $\overline{P}_m$, it will be referred to as estimated motor output power in this paper. The average frictional losses of the flapping mechanism can be obtained by,

$$\overline{P}_{friction} = \frac{1}{T}\int_T F\mu r_e \dot{\theta} dt. \quad (18)$$

The averaged aerodynamic power can be determined by,

$$\overline{P}_{aero} = \frac{1}{T}\int_T \dot{\beta}\overline{D}\overline{r} dt. \quad (19)$$

The experiments in three conditions of wingless, in a vacuum and in the air allowed attributing power to aerodynamic power, inertial power and power loss [14]. The estimated motor output power of the wingless system is attributed to the losses of the system. The difference between the estimated motor output power of the wingless case and those in a vacuum is attributed to the system's inertia in [14]. However, it should be noted that although the increase in the estimated motor output power for the case tested in a vacuum compared to the wingless case is due to adding wings inertia, the average estimated motor output power that is used to overcome inertia loads is zero. The inertia forces are conservative forces and their inclusion would not increase averaged power (active power) but the instantaneous power (active and reactive power). However, the increase in averaged mechanical power of the system can be attributed to the increased losses in the system due to increased internal loads. This difference is used here to estimate the effective friction coefficient μr_e. Similarly, the increase in estimated motor output power when tested in the air compared to the test in a vacuum is due to aerodynamic power requirements and increased losses due to further increase in internal forces.

The response of the system is obtained numerically using a model based on equations (1)–(14) in MATLAB Simulink. Equations (15), (17) and (18) are used in an iterative way to estimate the unknown parameters of the system. An initial guess for μr_e was chosen by assuming a half of the motor output power was used to overcome frictional losses when operating in the air for a rated voltage of 3 V. The initial guess for C_α was chosen by assuming the maximum angle of attack, α of 45° when the instantaneous lift was the maximum. Thereafter, they are adjusted through an iterative process to fit the estimated motor output curve in figure 5. The parameters used for the system are given in table 2. The comparison between simulations and measurements for electrical input power and estimated motor output power in three different conditions are shown in figures 4 and 5, respectively. Lift comparison is also provided in figure 6. It can be observed that the model can capture the dynamics of the system with high accuracy.

Table 2. Parameters used for modelling the flight mechanism and wings.

Parameter	Input value
r_c	5 mm
l	20 mm
H	6 mm
J_w	7.205×10^{-8} kg m^2 [14]
C_α	5×10^{-3}
μr_e	2.5×10^{-3} m

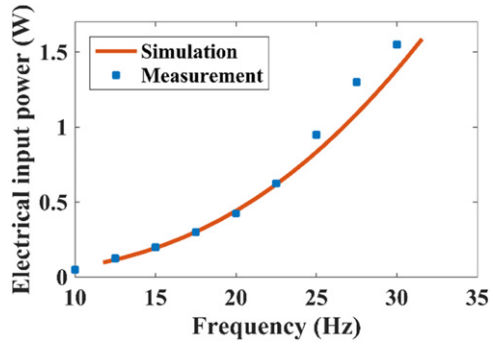

Figure 4. The average electrical input power, $\overline{P}_e$, as a function of flapping frequency.

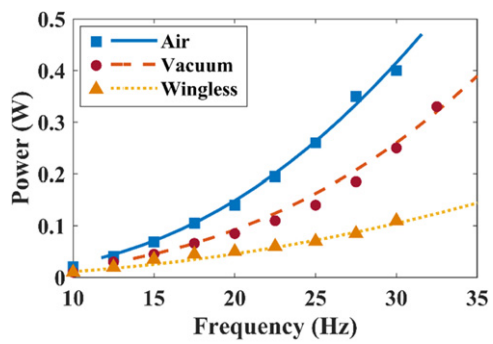

Figure 5. Comparison between measurements and simulation results for the estimated motor output power (equation (17)) required to drive the mechanism under different operating conditions as a function of flapping frequency. Measurements: markers, simulation: lines.

The model allows comparison between the power used to overcome aerodynamic loads and losses in the system. The electrical input power (equation (15)) and the motor output power (equation (16)) for the FWMAV driven in the air, in a vacuum and wingless condition as a function of frequency are shown in figure 7. The power loss of the system can be deduced from the difference between the input power and the aerodynamic power for the FWMAV operating in the air,

$$\overline{P}_{loss} = \overline{P}_e - \overline{P}_{aero}, \quad (20)$$

where $\overline{P}_{loss}$ is the total losses of the system.

The total loss of the system, $\overline{P}_{loss}$ is shown in figure 7(a) with the dashed line. The majority of the electrical input power is used to overcome system

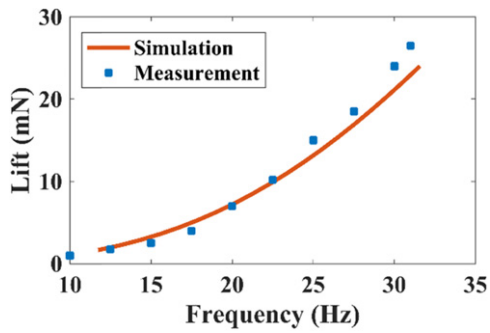

Figure 6. The lift as a function of the flapping frequency.

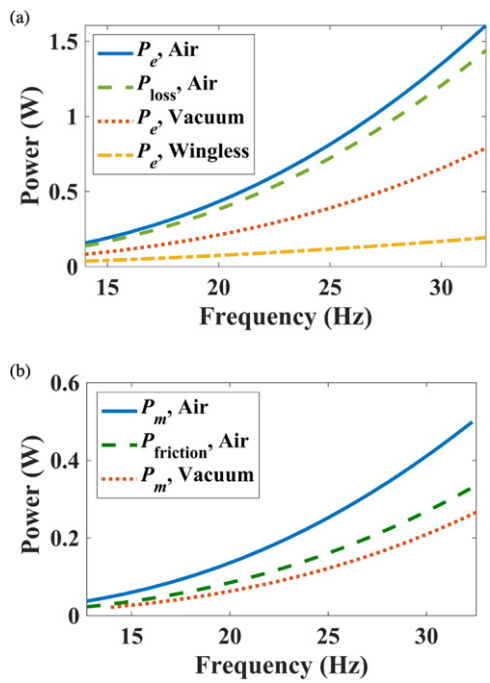

Figure 7. The total system losses and the transmission loss are compared with electrical input power and the motor out power as a function of frequency for three conditions of operating in the air, in a vacuum, and wingless. (a) The averaged electrical input power, $\overline{P}_e$. (b) The averaged motor output power, $\overline{P}_m$.

losses. This is due to the low efficiency of the DC motor at such a small scale and also high frictional losses in the flapping mechanism. For the wingless case and in a vacuum, the average electrical input power has been used solely to overcome system losses. For the system without wings, the crank reaction force is the minimum which results in the lowest level of losses in the system. By adding the wings and operating in a vacuum, the system losses are increased compared to the wingless case. This is due to the increased contact force F which increases the frictional losses of the system as well as increased motor losses due to the increased load. When the FWMAV is operating in the air, the aerodynamic loads would increase the crank reaction force F further which results in the increase of the friction losses shown in figure 7(b). The increased load also increased the motor losses which again can be seen as an increased total loss in figure 7(a).

The frictional loss $\overline{P}_{\text{friction}}$ of the transmission is shown in figure 7(b) alongside motor output torque for the FWMAV operating in the air and in a vacuum. The difference between the motor output torque and the frictional losses are equivalent to the aerodynamic power. It can be seen that the inclusion of the aerodynamic power would result in an additional energetic requirement caused by increased losses on the mechanism. To have a flying machine at a small scale the losses of the system should be reduced which requires decreasing contact forces on hinges. This can be achieved by adding an elastic element to the system and forming a resonant oscillator which is examined in the next section.

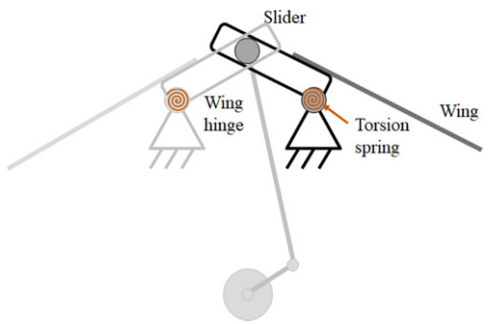

Figure 8. A schematic view of the flying mechanism with the addition of torsional springs.

4. The effect of the addition of torsion spring

Adding springs at the wing hinges can help a FWMAV to improve its efficiency by utilizing potential energy [5, 28, 29]. A schematic diagram of the flapping-wing mechanism with springs is shown in figure 8.

The equation of motion of the flapping system can be modified to include the effect of the springs,

$$J_w\ddot{\beta} + \overline{D}\overline{r} + k\beta = FH\left(\sin\gamma\tan\beta + \cos\gamma\right), \quad (21)$$

where k is the rotational stiffness of the springs.

Assuming a linear oscillator, the stiffness of the springs may be set to have resonance at the flapping frequency,

$$k = J_w\left(2\pi f_s\right)^2, \quad (22)$$

where f_s is the flapping frequency obtained using the mean velocity of the gear. A stiffness, k, of 1.377×10^{-3} N m^{-1} would result in a natural frequency of 22 Hz in the model used here. This is the average angular velocity of the motor at the rated voltage of 3 V. The effects of incorporating springs on the electrical input power and motor output power are shown in figure 9.

Generally, adding springs allows the system to operate in the same mean frequency with lower input

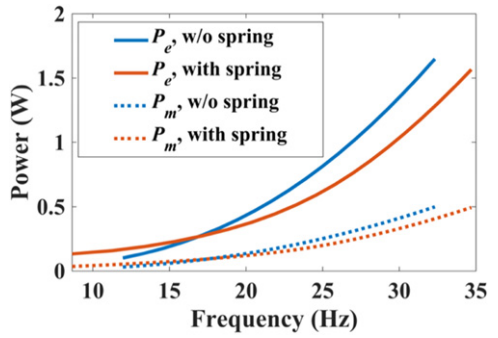

Figure 9. The effect of the addition of torsional springs on the averaged electrical input power requirement and the motor output power.

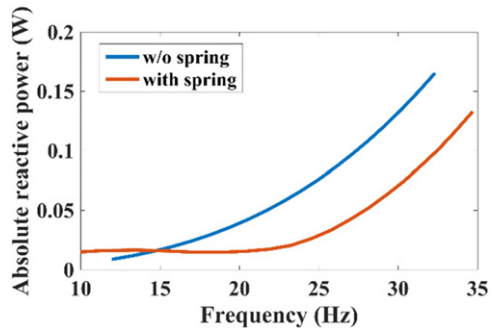

Figure 10. The mean absolute reactive power, $\overline{P}_{\mathrm{re}}$ of the system with and without springs.

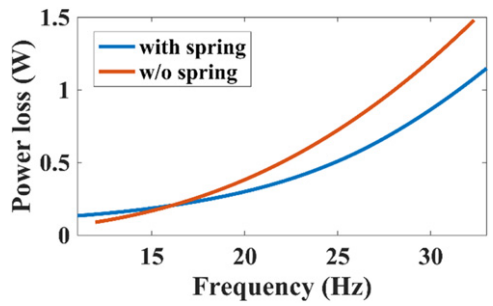

Figure 11. The average estimate of power losses on the transmission with and without springs.

power. However, the addition of the spring would increase the required power at low frequencies below 17 Hz.

Power that is transmitted to the load in part of a cycle and is retrieved from the load in another part of the cycle in a way that the net transferred power on average between the source and the load is zero is called reactive power. In an oscillatory mechanical system, reactive power would accelerate masses and deform elastic elements of the system [33]. The inertia and elastic forces can be used to obtain the average of absolute reactive power,

$$\overline{P}_{\mathrm{re}} = \frac{1}{T}\int_T \left|\left(J_{\mathrm{w}}\ddot{\beta} + K_{\mathrm{w}}\beta\right)\dot{\beta}\right| \mathrm{d}t, \tag{23}$$

where $\overline{P}_{\mathrm{re}}$ is the estimate of reactive power.

At low frequencies inertia loads are too small to cancel the spring forces and the motor should compensate those forces which cause an increase in reactive power of the system as shown in figure 10. At about 22 Hz the reactive power reaches its lowest value, but it would not become zero as one would expect from a linear oscillator which is due to the nonlinearities in the system. The total power loss in the system is shown in figure 11 for two cases of the system without spring and with spring which shows how adding spring can reduce the system losses by reducing internal forces in the system at higher frequencies. At frequencies higher than the tuning frequencies, spring still would cancel inertia load partially and would reduce the energetic requirements. It can be shown through figures 9–11 that the mathematical model considering friction forces is able to capture the effect of incorporating springs in the model. Not only the change of the absolute reactive power on the system but also the reduction of input power and losses on the system are observed which cannot be explained by a model treating losses as a viscous damper or a quadratic damper.

To scrutinise the efficiency of the system, the measure for efficiencies of the system, η_{system}, motor, η_{motor}, and mechanism, η_{mech}, are introduced,

$$\eta_{\mathrm{system}} = \frac{\overline{P}_{\mathrm{aero}}}{\overline{P}_{\mathrm{e}}} \tag{24}$$

$$\eta_{\mathrm{motor}} = \frac{\overline{P}_{\mathrm{m}}}{\overline{P}_{\mathrm{e}}} \tag{25}$$

$$\eta_{\mathrm{mech}} = \frac{\overline{P}_{\mathrm{aero}}}{\overline{P}_{\mathrm{m}}}. \tag{26}$$

Incorporating springs increases both efficiencies of motor and mechanism in general as shown in figure 12. Springs reduce the reactive power of the system by saving and releasing potential energy in each stroke. Since the spring stiffness is set to have resonance at 22 Hz, the mechanism efficiency is maximised at 22 Hz. Similarly, the maximum efficiency of the system is observed at approximately 21 Hz which is between the frequencies of the maximum efficiency of motor and mechanism. Such a small DC motor has very low efficiency due to its coreless structure with high electromagnetic losses. Furthermore, the friction losses in the motor bearings can be relatively high at small scales. Although the flapping mechanism has a varying load, the DC motor achieves 30% efficiency reported by the manufacturer at the rated voltage and under constant load. There is a slight improvement in motor efficiency when it is used in the FWMAV with added springs.

The addition of the springs also helps the system to generate more lift at the same averaged frequency

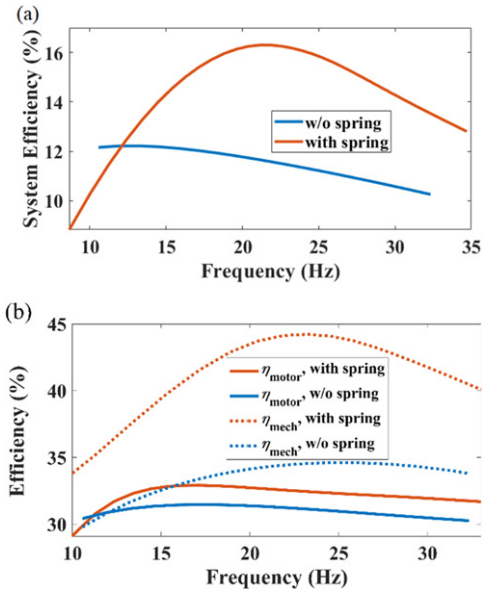

Figure 12. (a) The efficiency of the system with and without springs and (b) the efficiency of the motor and flight mechanism with and without springs.

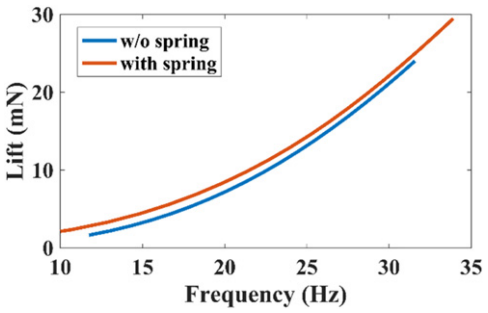

Figure 13. The effect of the addition of torsional springs on the generated lift.

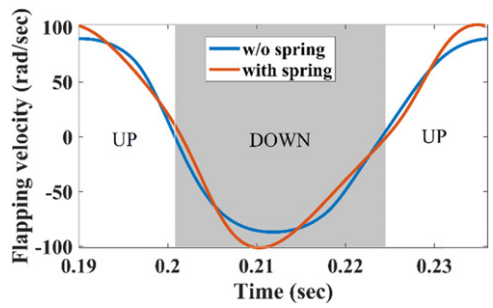

Figure 14. The instantaneous flapping velocity with and without spring at 22 Hz, DOWN and UP indicate the direction of the slider.

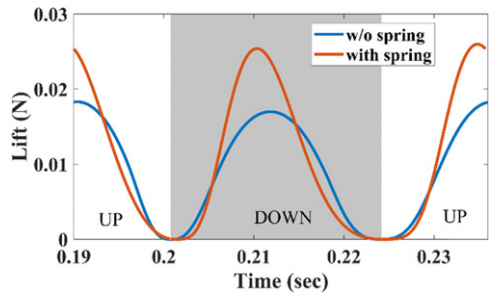

Figure 15. Instantaneous lift with and without spring at 22 Hz.

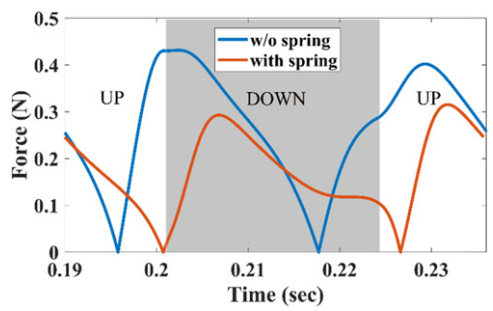

Figure 16. The instantaneous crank reaction force with and without spring at 22 Hz.

as shown in figure 13. Despite the same mean frequency, the addition of springs causes a reduction in the fluctuation of the motor speed and an increase in the maximum amplitude of wing stroke velocity. The increased wing stroke velocity results in a higher lift. The increase of wing stroke velocity also increases wing rotation, resulting in a larger lift. Thus, the average lift would be higher while the friction losses are lower at the same mean frequency compared to the original system without springs.

The instantaneous flapping velocity at approximately 22 Hz is shown in figure 14 for the system with and without spring. The maximum velocity is 14.2% higher for the system with spring. The instantaneous lift is shown in figure 15 at the same frequency. The maximum instantaneous lift increases by about 39.9% (from 18.3 to 26.0 mN). The instantaneous crank reaction force at 22 Hz is shown in figure 16. Its maximum decreases approximately by 27.1% (from 0.432 to 0.315 N) by incorporating springs. At this frequency, the average lift and efficiency increase approximately 15.4% and 4.7%, respectively.

Furthermore, at frequencies above 17 Hz, the benefit of adding spring is even more when lift and losses are compared for the same applied voltage. The instantaneous lift is compared for the two systems at the rated voltage of 3 V in figure 17. The flapping frequency is about 21.7 Hz for the system without spring and approximately 23.3 Hz for the system with spring. The instantaneous wing angular velocity and crank reaction force is shown in figures 18 and 19. Springs allow the system to achieve 33.3% higher mean lift by increasing the maximum wing angular velocity of 19.7% at this voltage. The average force is also reduced on the hinge by 33% at the rated voltage.

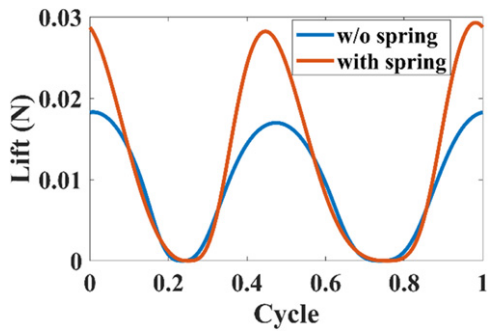

Figure 17. The instantaneous lift for a cycle with and without spring at 3 V.

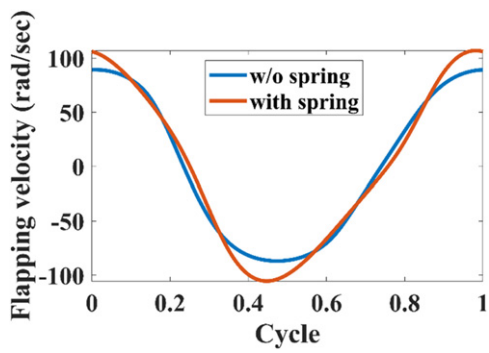

Figure 18. The instantaneous flapping velocity for a cycle with and without spring at 3 V.

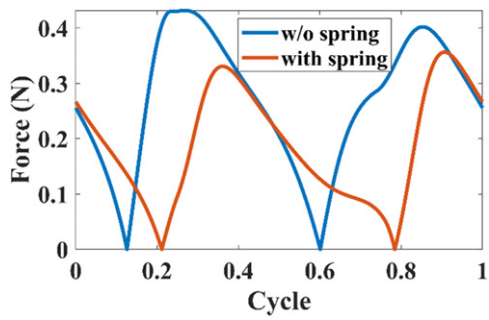

Figure 19. The instantaneous crank reaction force for a cycle with and without spring at 3 V.

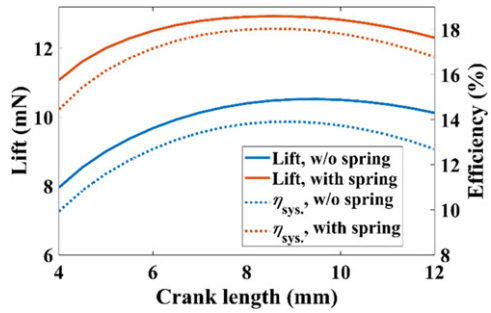

Figure 20. The lift and the efficiency of the system as a function of the crank length with and without springs.

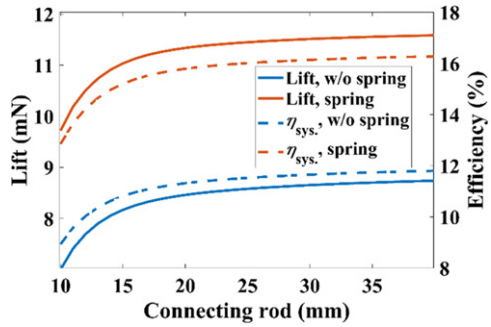

Figure 21. The lift and the efficiency of the system as a function of the length of the connecting rod with and without springs.

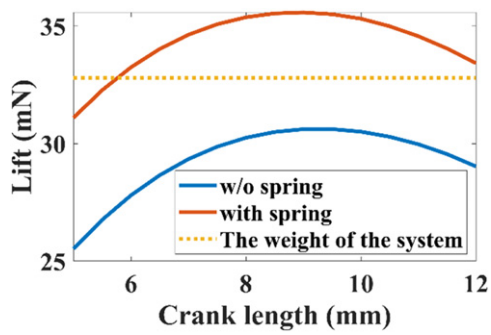

Figure 22. The generated lift as a function of the length of the crank with and without torsional springs and at higher input voltage of 5 V. The dashed orange line indicates the weight of the system.

5. Optimisation

The generated lift and the system efficiency should increase for a flying machine simultaneously. To optimise the system, trend analysis was conducted at the rated input voltage of 3 V. The length of the crank and connecting rod are varied while the wings and motor remain the same. With the fixed connecting rod of 20 mm, the lift and efficiency are maximised with the crank length of 9 mm as shown in figure 20. The addition of springs increases the lift and the system efficiency, and an increase in the crank length similarly affects the system with springs. In choosing the appropriate length, it is important to note that a longer rod would increase the overall mass of the system which is undesirable. A longer connecting rod tend to allow larger lift and higher efficiency with the fixed crank length of 5 mm for both the system with springs and without springs, which is shown in figure 21. However, the increases of both lift and efficiency by the increase of the connecting rod are moderate for a connecting rod with a length larger than 20 mm.

The mass of the flapping system is reported to be 3.34 g [14], thus, the lift should be larger than 32.8 mN to allow hovering. However, even the maximum lift with an input voltage 3 V does not satisfy

this requirement. Once parameters are determined, the input voltage is the sole control variable that determines the operating frequency of the system. The maximum available input voltage is assumed to be 5 V in this research while the rated voltage of the motor is 3 V. Even though higher voltage generates higher lift, the system cannot obtain enough lift without springs as shown in figure 22. The lift can increase up to 35.6 mN by adjusting the length of the crank and adding torsional springs.

6. Conclusion

This paper provides a mathematical model of a FWMAV including the electromechanical model of a commercial DC gear motor and the mechanical model of a flapping mechanism. The parameters of the system are estimated based on the published data and the simulation results show that the model can capture the real response of the system with a good accuracy. In a reciprocating system, reactive power is inevitable because of the inertial loads. Although the kinetic energy storage capacity of the motor would provide a means to compensate for the reactive power requirements, the increased internal loads cause an increase in power losses. Modelling friction forces allows the prediction of the system losses and power requirements for different operational conditions.

The model also makes it possible to investigate the effect of adding springs on power requirements and lift generation. Adding springs at wing hinges reduces the effect of wing moment of inertia by saving and releasing potential energy in each cycle. Consequently, the average electrical input power reduced approximately by 18% at 22 Hz whilst the average lift and the system efficiency increase by about 15.4% and 4.7% at 22 Hz, respectively while the maximum instantaneous lift increases by about 39.9%. It shows that springs help the system to be more efficient and to generate larger lift with the same input power. Lastly, through the trend analysis, an optimised crank and connecting rod lengths are suggested to 9 mm and 20 mm, respectively. The optimum operating ranges are also suggested by estimating the lift and the efficiency of the system. With the parameters introduced in this paper, the system can have the best efficiency at the range from 10 Hz to 17 Hz without spring and from 18 Hz to 25 Hz with spring. However, only the model with springs and a 9 mm crank length can generate enough lift at an input voltage of 5 V to support its weight.

The analysis demonstrates the effect of the low efficiency of a DC motor at such a small scale on the system performance. Furthermore, the flapping mechanism would have relatively high frictional losses. However, DC motors are one of the most common type of actuators and the efficiencies of the motors and the flapping mechanisms can be improved by employing advanced manufacturing techniques in a commercial setting. The performance of the FMWAV should be compared with a similar system using direct drive actuators in future studies.

Data availability statement

All data that support the findings of this study are included within the article. The MATLAB Simulink model and its corresponding m-file for this study are available at the following DOI: https://doi.org/10.5522/04/17295395.v1.

ORCID iDs

Moonsoo Park https://orcid.org/0000-0001-6165-5295

Reference

[1] Wood R J 2007 Liftoff of a 60 mg flapping-wing MAV *IEEE RSJ Int. Conf. Intell. Robot. Syst.*
[2] Keennon M, Klingebiel K and Won H 2012 *50th AIAA ASM Including the New Horizons Forum and Aerospace Exposition*
[3] Gerdes J *et al* 2014 *Soft Robot.* **1** 275–88
[4] Tay W B, van Oudheusden B W and Bijl H 2015 *J. Fluids Structures* **55** 237–61
[5] Bolsman C T 2010 *PhD Thesis* University of Delft, Delft
[6] Pornsin-Sirirak T N, Tai Y C, Ho C M and Keennon M 2001 *Proc. NASA/JPL Workshop on Biomorphic Robotics* vol 14
[7] Hsiao F Y, Yang L J, Lin S H, Chen C L and Shen J F 2012 *IEEE Control Syst.* **32** 35–48
[8] Azhar M, Campolo D, Lau G K, Hines L and Sitti M 2013 *Proc. IEEE Int. Conf. Robot. Autom.* pp 1397–402
[9] Mukherjee S and Ganguli R 2012 *Int. J. Smart Nano Mater.* **3** 103–22
[10] Yang L-J, Esakki B, Chandrasekhar U, Hung K-C and Cheng C-M 2015 *Int. J. Micro Air Vehicles* **7** 181–202
[11] Chen C and Zhang T 2019 *Micromachines* **10** 144
[12] Zhang C and Rossi C 2017 *Bioinspir. Biomim.* **12** 025005
[13] Kok J M and Chahl J S 2015 *Proc. PROC SPIE* **9429** 94290L
[14] Lau G-K, Chin Y-W, Goh J T-W and Wood R J 2014 *IEEE Trans. Robot.* **30** 1187–97
[15] Weis-Fogh T 1972 *J. Exp. Biol.* **56** 79–104
[16] Ansari S A, Żbikowski R and Knowles K 2006 *Prog. Aerosp. Sci.* **42** 129–72
[17] Mouret J-B, Doncieux S and Meyer J-A 2006 *Proc. 9th Int. Conf. Simulation of Adapt. Behav.* pp 606–18
[18] Galiński C and Żbikowski R 2007 *Mater. Design* **28** 783–96
[19] Sepcu L C 2012 *Int. Conf. Applied and Theoretical Electricity (ICATE)* pp 1–4
[20] Campolo D, Azhar M, Lau G K and Sitti M 2014 *IEEE ASME Trans. Mechatron.* **19** 109–20
[21] Baek S S, Ma K Y and Fearing R S 2009 *IEEE RSJ Int. Conf. Intell. Robot. Syst.* 2854–60
[22] Khan Z, Steelman K and Agrawal S 2009 *IEEE Int. Conf. Robot. Autom.* 3651–6
[23] Jeon J, Cho H, Kim Y, Lee J, Gong D, Shin S and Kim C 2017 *Int. J. Micro Air Vehicles* **9** 253–69
[24] Zhang J, Cheng B, Roll J A, Deng X and Yao B 2013 *IEEE Int. Conf. Robot. Autom.* pp 4029–34
[25] Khan Z A and Agrawal S K 2006 *Proc. IEEE Int. Conf. Robot. Autom.* pp 2323–8
[26] Lynch J, Gau J, Sponberg S and Gravish N 2021 *J. R. Soc. Interface* **18** 20200888
[27] Alexander R M and Bennet-Clark H C 1977 *Nature* **265** 114–7
[28] Madangopal R, Khan Z A and Agrawal S K 2005 *J. Mech. Des.* **127** 809–16

[29] Tantanawat T and Kota S 2007 *J. Mech. Des.* **129** 1064–75
[30] Park M, Abolfathi A, Biggs J D and Ventikos Y 2018 *Proc. ISMA*
[31] Precision Microdrives Product data sheet nano planetary™ 6 mm DC gearmotor-16 mm type https://catalogue.precisionmicrodrives.com/product/datasheet/206-102-6mm-dc-gearmotor-16mm-type-datasheet.pdf
[32] Dickinson M H, Lehmann F-O and Sane S P 1999 *Science* **284** 1954–60
[33] Abolfathi A 2018 *MATEC Web Conf.* **148** 03007